ATR-FTIR spectroscopy reveals polycyclic aromatic hydrocarbon contamination despite relatively pristine site characteristics: results of a field study in the Niger Delta

Blessing E. Obinaju and Francis L. Martin[*]

Lancaster Environment Centre, Lancaster University, Bailrigg, Lancaster LA1 4YQ, UK

Corresponding author: Prof Francis L. Martin PhD, Centre for Biophotonics, LEC, Lancaster University, Lancaster LA1 4YQ, UK; Tel.: +44(0)1524 510206; Email: f.martin@lancaster.ac.uk
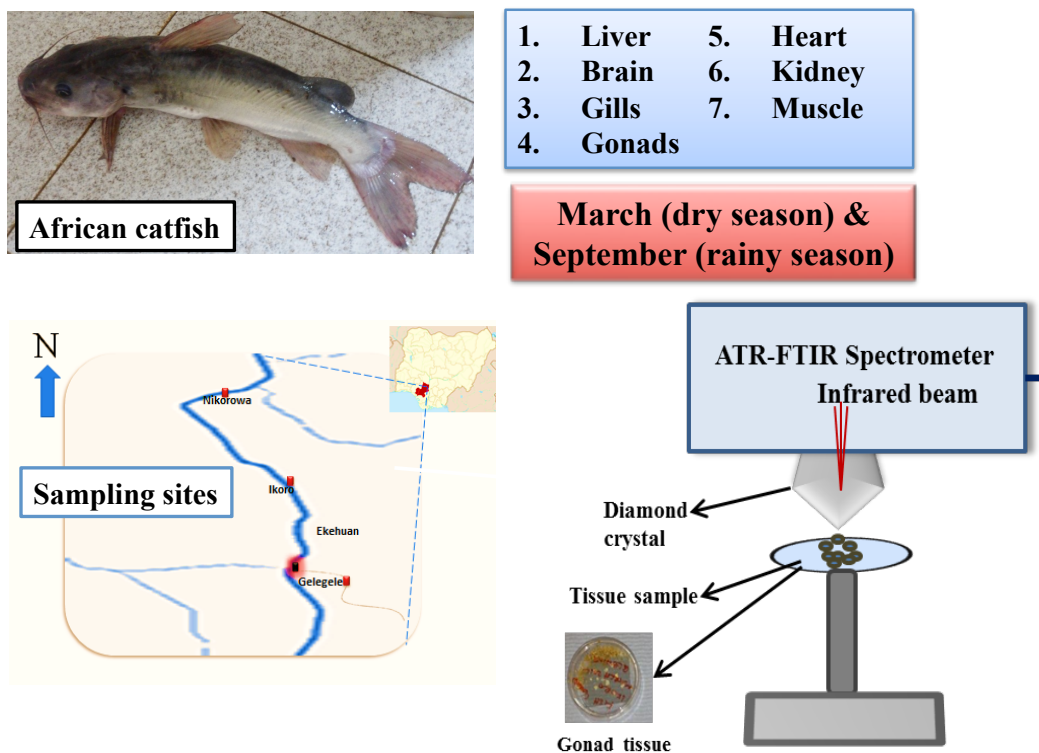
Abstract

Fourier-transform infrared (FTIR) spectroscopy is an emerging technique to detect biochemical alterations in biological tissues, particularly changes due to sub-lethal exposures to environmental contaminants. We have previously shown the potential of attenuated total reflection FTIR (ATR-FTIR) spectroscopy to detect real-time exposure to contaminants in sentinel organisms as well as the potential to relate spectral alterations to the presence of specific environmental agents. In this study based in the Niger Delta (Nigeria), changes occurring in fish tissues as a result of polycyclic aromatic hydrocarbon (PAH) exposure at contaminated sites are compared to the infrared (IR) spectra of the tissues obtained from a relatively pristine site. Multivariate analysis revealed that PAH contamination could be occurring at the pristine site, based on the IR spectra and significant ($P <0.0001$) differences between sites. The study provides evidence of the IR spectroscopy techniques' sensitivity and supports their potential application in environmental biomonitoring.

Highlights

- Spectral alterations point to sub-lethal exposures to environmental contaminants
- Biospectroscopy detects real-time exposures to contaminants in sentinel organisms
- Field study based in the Niger Delta (Nigeria)
- PAH contamination occurs at a pristine site, determined by IR spectra
- Biospectroscopy has potential applications in environmental biomonitoring

ToC graphic

African catfish

1. Liver	5. Heart
2. Brain	6. Kidney
3. Gills	7. Muscle
4. Gonads	

March (dry season) & September (rainy season)

Sampling sites

Nikorowa

Ikoro

Ekehuan

Gelegele

ATR-FTIR Spectrometer
Infrared beam

Diamond crystal

Tissue sample

Gonad tissue

1. Introduction

Human activities generate potentially toxic compounds, some with unusual characteristics. Most of these compounds end up in various parts of the ecosystem and constitute a degree of hazard to biological populations including humans. Synthetic chemicals and materials such as petroleum hydrocarbons, persistent organic pollutants (POPs), pesticides and metals which mostly contaminate aquatic systems, are more often linked to advancements in industrialization (Li et al., 2001; Zhang et al., 2005). Exposures to these compounds have been linked to a variety of adverse effects including neurodevelopmental alterations following *in utero* exposure (Perera and Herbstman, 2011; Perera et al., 2006; Wormley et al., 2004).

Studies continue to show that chemical contaminants are capable of inducing toxicity in organisms, even at very low concentrations (Kalantzi et al., 2004; Pang et al., 2012; Ukpebor et al., 2011), and their accumulation in the tissues of organisms post-exposure, particularly aquatic and wildlife species, generates concern for the possibility of contaminant transfer through the food chain (Gwaski et al., 2013; Lozano et al., 2012). Several analytical techniques exist to biomonitor contaminants in the ecosystem and within organisms. In recent years, the field of biospectroscopy, a technique that employs the use of infrared (IR) spectrometry or the coupling of IR spectrometry to other techniques (*e.g.*, microscopy [IR microspectroscopy]) to understand changes in cells and tissues, especially those that occur as a result of exposure to environmental chemicals, has gained immense attention. The application of biospectroscopy to observe these changes is based on the knowledge of the vibrational modes of biomolecules, which generates spectral information [often known as the "biochemical-cell fingerprint" (biofingerprint)] when exposed to IR radiation (Martin et al., 2010). Based on changes to the biofingerprint, it is possible to distinguish between cell/tissue types (German et al., 2006) with potential cell characterization (Pijanka et al., 2013).

Biospectroscopy techniques are non-destructive to samples, relatively reagent-free and can generate rapid, high-throughput and robust results in real-time with high sensitivity to minimal changes within biomolecules (Martin et al., 2010). Thus, biospectroscopy can be employed to study contaminant-induced responses in organisms, using a wide variety of sample types. Particularly, it has the potential to biomonitor environmental contaminants in most sentinels, in real-time (Ibrahim et al., 2012; Llabjani et al., 2012; Malins and Gunselman, 1994; Obinaju et al., 2014). These techniques can be optimised for even more applications (Baker et al., 2014). Biospectroscopy techniques involving the use of attenuated total reflection Fourier-transform infrared (ATR-FTIR) spectroscopy require minimal sample preparation (Martin et al., 2010; Obinaju and Martin, 2013) and have been shown to detect the slightest chemical-induced variation in samples at very low ($<10^{-9}$ M) concentration ranges (Ahmad et al., 2008; Llabjani et al., 2014; Llabjani et al., 2011; Ukpebor et al., 2011).

We have previously shown that ATR-FTIR spectroscopy is able to differentiate between real-time exposure effects both animal and plant tissues from sites with varying degrees of environmental contamination (Obinaju et al., 2014). Herein, we compare tissues of the African Catfish (*Heterobrachus bidorsalis*) from sites with a known history of polycyclic aromatic hydrocarbon (PAH) contamination, to samples from a relatively pristine site with no documented history of contamination and no industrial activity. Our aim was to determine if we could signature PAH-induced toxicity in fish tissues using ATR-FTIR spectroscopy.

2. Materials and Methods

Samples of *Heterobrachus bidorsalis* were collected in March 2013 by local fishermen at Gelegele, Ikoro and Ifiayong in Edo and Akwa Ibom States, within the Niger Delta region. Only wild fish of similar range of weight and length, classified as neither fingerlings nor juvenile, were used. Site descriptions as well as sample handling, tissue pre-processing methods and spectral measurements have been previously detailed (Obinaju et al., 2014).

Briefly, each site was selected based on the documented knowledge of industrial activities, which yield possible environmental contaminating compounds. Gelegele and Ikoro are located in close proximity to petroleum exploration activities and Ifiayong is a rural fishing community with no documented history of petroleum exploration or similar industrial type activities. Each excised fish tissue was thinly sliced ($\leq$1-mm thick/slice) by hand using a Stadie-Riggs handheld microtome and Thomas blade (Taylor et al., 2011). Each slice was rehydrated by washing twice in dH_2O. Sample slices were mounted on Low-E reflective glass slides (Kevley Technologies, Chesterland, OH), allowed to air-dry and desiccated for a minimum of 24 h prior to interrogation using ATR-FTIR spectroscopy.

2.1 Spectral acquisition and pre-processing

IR spectra were obtained using a Bruker Vector 27 FTIR spectrometer with Helios ATR attachment containing a diamond crystal (Bruker Optics Ltd., Coventry, UK). Data acquired for each experimental condition (*i.e.*, each sample slide) consisted of 10 spectra, each from a random area of the tissue slice under interrogation, using an FTIR imaging system coded for 32 scans per spectra and 3.84 cm^{-1} spectral resolution. The ATR crystal was cleaned with dH_2O, dried thoroughly and a new background spectrum taken prior to analysis of a new sample. Raw spectra were acquired in the 4000 cm^{-1} - 400 cm^{-1} range. Spectra in the region of interest (1800 - 900 cm^{-1}) were selected and pre-processed (rubberband baseline corrected and normalized to Amide I peak) to account and correct for noise, sloping baseline effects, differences in sample thickness or concentration.

2.2 Computational analysis

Multivariate analysis [principal component analysis-linear discriminant analysis (PCA-LDA)] were performed in MATLAB R2011b using an in-house developed IRTools toolbox (Trevisan et al., 2013). Results were visualized either as scores plots or cluster vectors plots;

the toolbox was set to identify the top six wavenumbers responsible for site differences. The mean band/peak area of the absorbance at specific regions was measured by calculating the integrated absorbance between the two wavenumbers (max-min) of the given region.

2.3 Statistical analysis

Variation in the tissues within the dataset was tested for statistical significance using Mann Whitney U-test, one-way analysis of variance ($ANOVA$) and Dunnett's multiple comparison tests, where the P-value of less than 0.05 ($P<0.05$) was considered statistically significant.

3. Results

Figs. 1 and 5A show the mean spectral absorbance for the brain, kidney, heart, liver and gill tissues of African catfish. Tissues showed relatively marked differences within the lipid ($\sim$1740 cm^{-1}), protein ($\sim$1700 cm^{-1} - 1400 cm^{-1}) and DNA/RNA ($\sim$1399 cm^{-1} - 900 cm^{-1}) regions of the biofingerprint for all tissues, excluding gills where very subtle alterations to only the DNA/RNA region were observed (Fig 5). Of note, most tissue (brain, liver, and gills) spectra sampled from Ifiayong seemed most consistent with tissues from Gelegele.

Using the first LDA factor (LD1) in a one-dimensional (1-D) scores plot, the degree of variation in tissues between the sampling sites was visualized, following the application of PCA-LDA (Figs. 2 and 5B). The tissues obtained from Ikoro seemed most different from the corresponding tissues from other sites and produced a positive index along the LD1 space in most tissues [brain, liver (Fig 2) and gill (Fig 5)]. The variation between sites was tested using one-way analysis of variance and Dunnett's multiple comparison test, comparing each site against the chosen reference site (Ifiayong). The variations between sites were significant with $P<0.0001$ in $ANOVA$ and $P<0.01$ in Dunnett's multiple comparison test for all tissues.

Cluster vectors plots (Figs. 3 and 4) show wavenumbers responsible for the segregation in scores plot, and each distinguishing wavenumber corresponding to specific

biochemical assignment (Table 1 and 2). Mean band areas were calculated for wavenumbers responsible for the differences in mean spectral absorbance. Peak centroids were observed to shift to higher or lower wavenumbers, with significant increase/decrease in the mean band areas (Table 3).
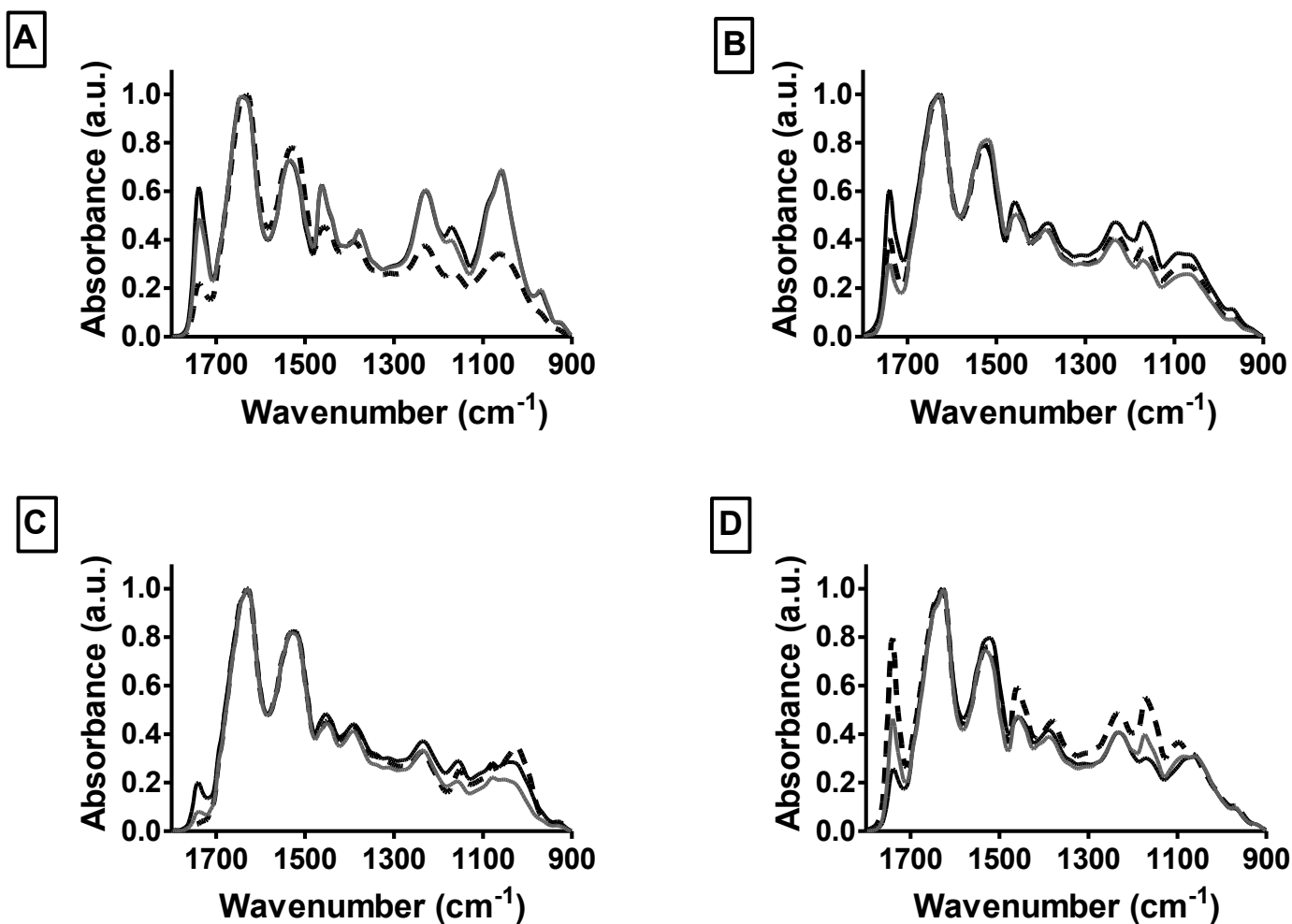
Fig 1. Mean spectra acquired from brain **(A)**; kidney **(B)**; heart **(C);** and, liver **(D)** tissues of the African catfish (*Heterobranchus bidorsalis)* obtained in March 2013 from sampling points Ifiayong (Ify), Ikoro (Iko) and Gelegele (Geg) in the Niger Delta region. Ify (solid black lines), Iko (broken black lines) and Geg (grey lines). Spectra were cut between 1800 and 900 cm^{-1}, rubberband baseline corrected and normalized to the Amide I peak (1650 cm^{-1}).
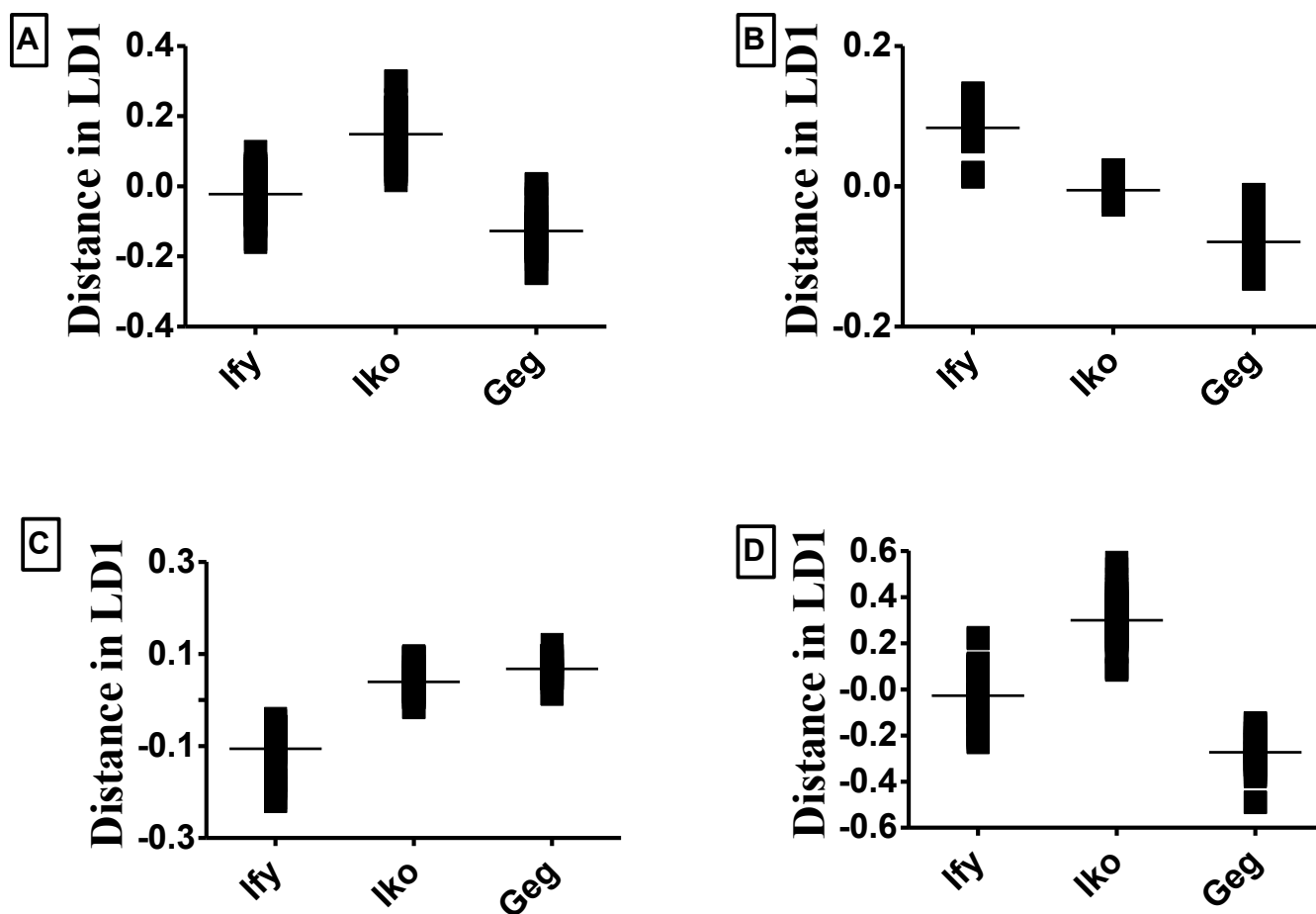
Fig 2. Principal component analysis coupled with linear discriminant analysis (PCA-LDA) values acquired from brain **(A)**; heart **(B)**; kidney **(C)**; and, liver **(D)** tissues of the African catfish (*Heterobranchus bidorsalis*) obtained in March 2013 from sampling points Ifiayong (Ify), Ikoro (Iko) and Gelegele (Geg) in the Niger Delta region. Spectra were cut between 1800 - 900 cm^{-1}, rubberband baseline corrected and normalized to the Amide I peak (1650 cm^{-1}). Normalized spectra were mean-centred before application of PCA-LDA. As determined using one-way ANOVA, PCA-LDA values in each class were significant (P <0.0001). Test classes (Geg, Iko) were significant (P <0.01) when compared to reference class (Ify) using Dunnett's Multiple Comparison Test.

Fig. 3. Cluster vectors plots acquired from brain **(A)**, heart **(B)**, kidney **(C)** and liver **(D)** tissues of the African catfish (*Heterobranchus bidorsalis)* obtained in March 2013 from sampling points Ifiayong (Ify), Ikoro (Iko) and Gelegele (Geg) in the Niger Delta region. Cluster vectors plots were derived using Ifiayong as reference site. Ify (solid black lines), Iko (broken black lines) and Geg (grey lines). Spectra were cut between 1800 - 900 cm^{-1}, rubberband baseline corrected, vector normalized and mean-centred before multivariate analysis (PCA-LDA).
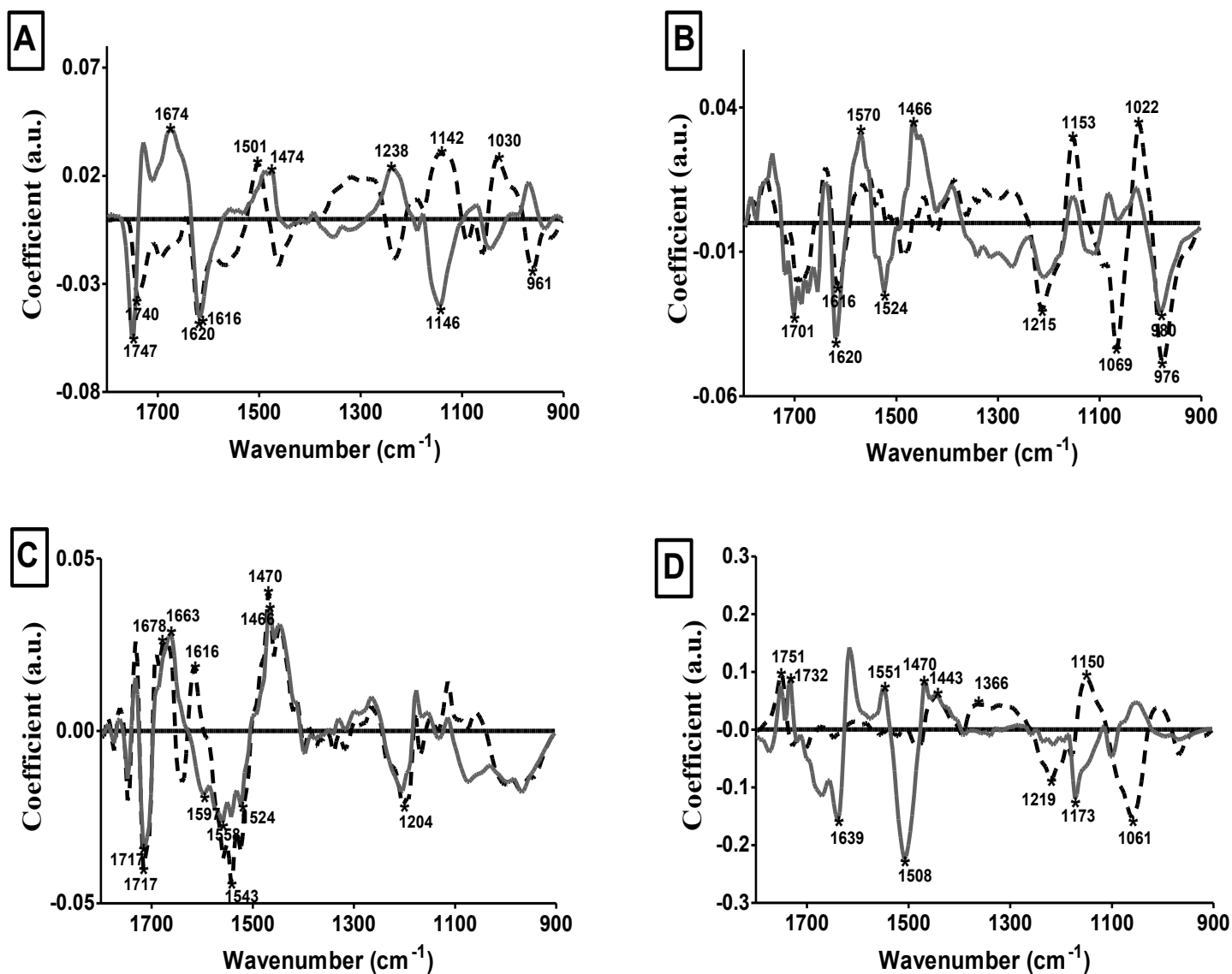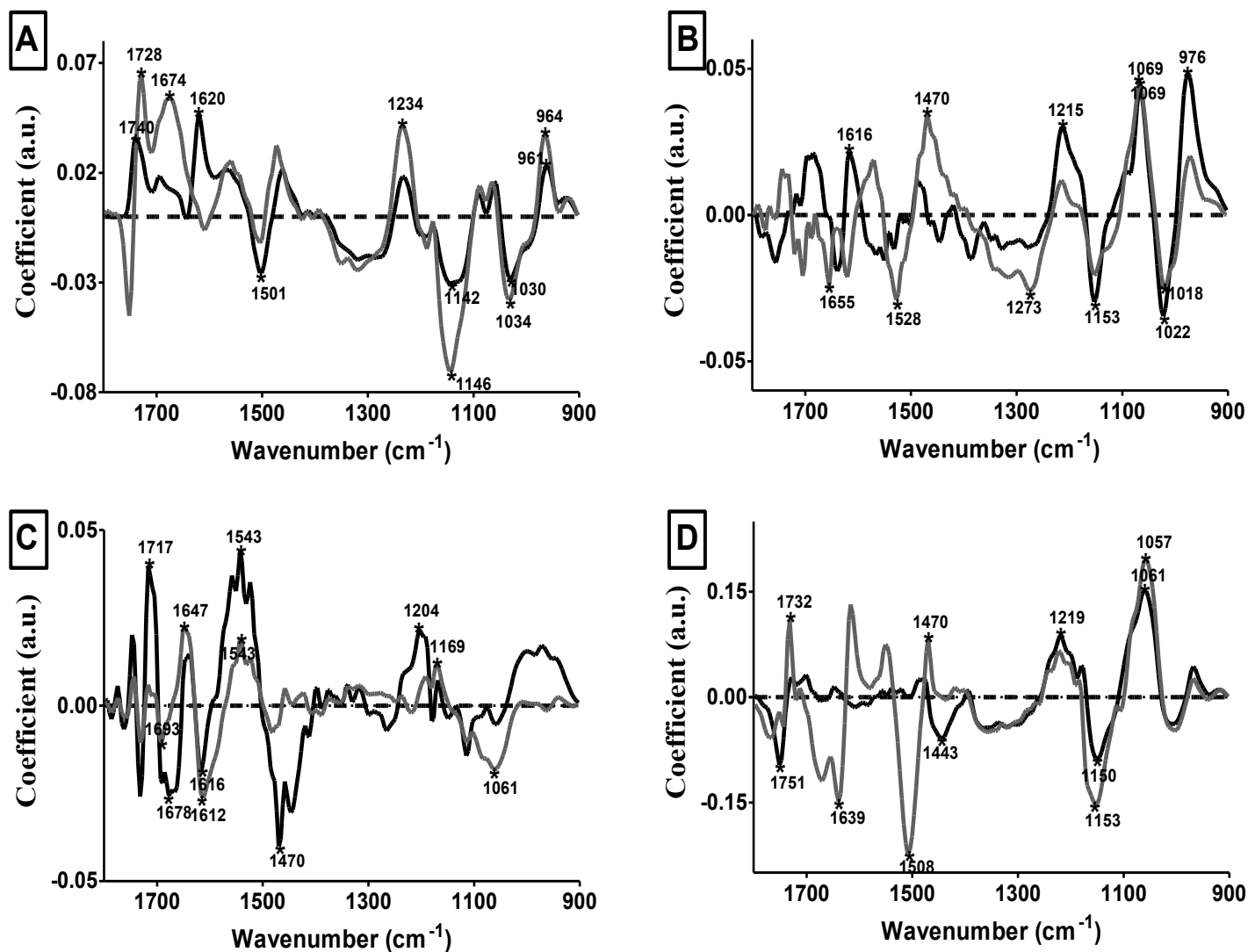
Fig. 4. Cluster vectors plots acquired from brain **(A)**; heart **(B)**; kidney **(C)**; and, liver **(D)** tissues of the African catfish (*Heterobranchus bidorsalis)* obtained in March 2013 from sampling points Ifiayong (Ify), Ikoro (Iko) and Gelegele (Geg) within the Niger Delta region. Cluster vectors plots were derived using Ikoro as reference site. Ify (solid black lines), Iko (broken black lines) and Geg (grey lines). Spectra were cut between 1800 - 900 cm^{-1}, rubberband baseline corrected, vector normalized and mean-centred before multivariate analysis (PCA-LDA).
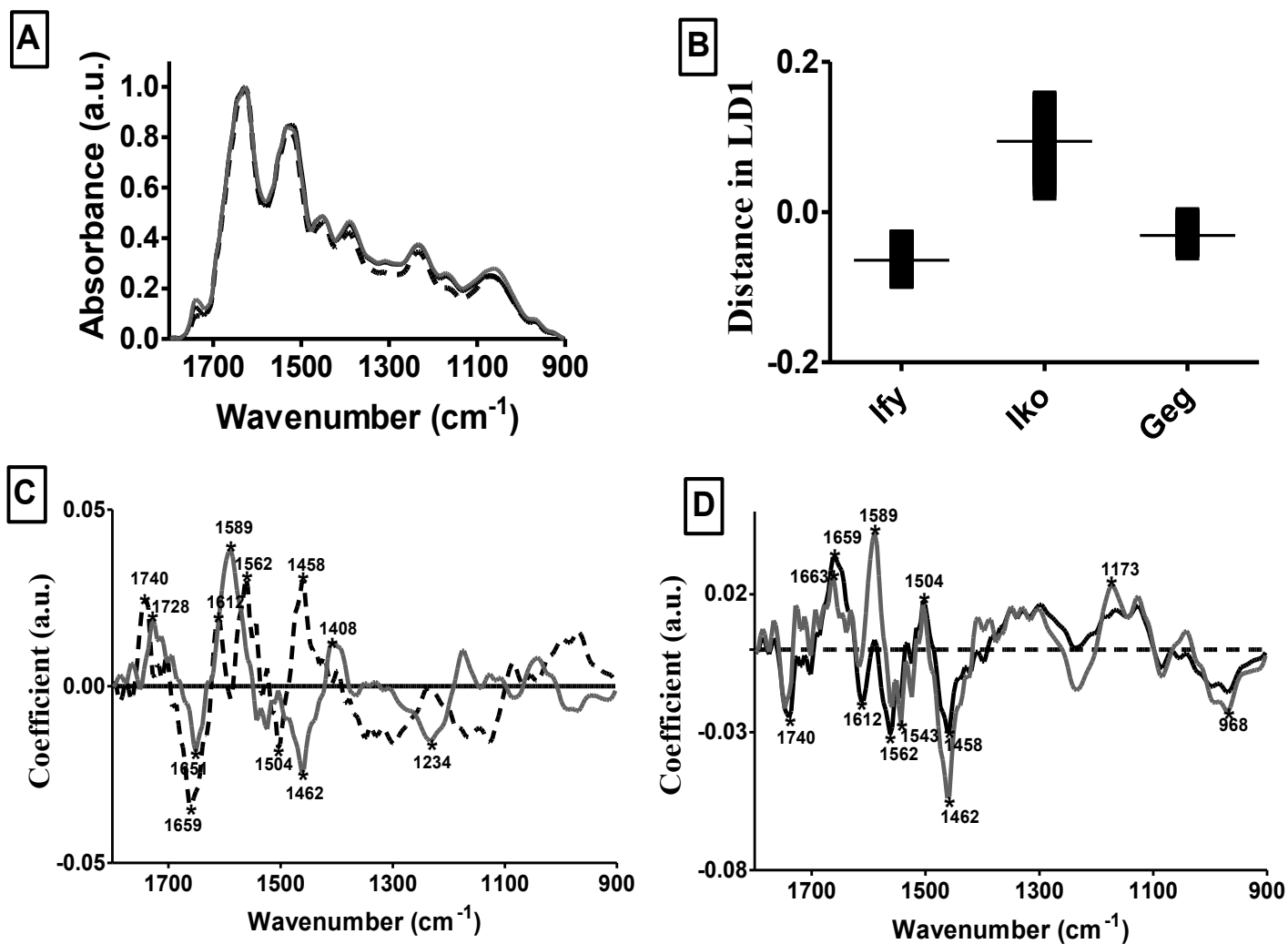
Fig. 5. Mean spectra **(A)**; principal component coupled with linear discriminant analysis (PCA-LDA) scores **(B)**; and, cluster vectors **(C & D)** plots acquired from gill tissues of the African catfish (*Heterobranchus bidorsalis)* obtained in March 2013 from sampling points Ifiayong (Ify), Ikoro (Iko) and Gelegele (Geg) within the Niger Delta region. Cluster vectors plots were derived using Ifiayong **(C)** and Ikoro **(D)** as reference sites. Ify (solid black lines), Iko (broken lines) and Geg (grey lines). Spectra were cut between 1800 - 900 cm^{-1}, rubberband baseline corrected, vector normalized and mean-centred before multivariate analysis (PCA-LDA). As determined using one-way ANOVA, the PCA-LDA values in each class were significant (P <0.0001). Test classes (Geg, Iko) were significant P <0.05 when compared to reference class (Ify) using Dunnett's Multiple Comparison Test.

Table 1 Attenuated total reflection Fourier-transform infrared (ATR-FTIR) spectroscopy distinguishing wavenumbers as shown in cluster vectors plots, and corresponding tentative chemical assignments: wavenumbers responsible for variance between tissue samples of the African catfish (*Heterobranchus bidorsalis)* obtained in March 2013 from sampling points Ifiayong, Ikoro and Gelegele in the Niger Delta region. Distinguishing wavenumbers were derived following multivariate analysis and using Ifiayong as reference site.

Sample	Site	Distinguishing wavenumbers (cm^{-1})	Tentative assignments	References
Brain	Ikoro	1740	>C=O ester stretching vibrations in triglycerides	3
		1620	Peak of nucleic acids due to the base carbonyl stretching and ring breathing mode	3
		1501	In-plane CH bending vibrations from phenyl rings	1
		1142	Phosphate and oligosaccharides; oligosaccharide C–O bond in hydroxyl group that might interact with some other membrane components	1
		1030	Glycogen vibrations; collagen and phosphodiester groups of nucleic acids; stretching C–O ribose.	1
		961	C–O deoxyribose.	1
	Gelegele	1747	C=O stretching vibrations of lipids, triglycerides, cholesterol esters	3
		1674	Anti-parallel β-sheet of Amide I, v(C=C) *trans*, lipids, fatty acids	1
		1616	Amide I (carbonyl stretching vibrations in side chains of amino acids)	3
		1474	Asymmetric CH$_3$ bending of the methyl group of proteins	1
		1238	Asymmetric PO$_2^-$ stretching	1
		1146	CO-O-C asymmetric stretching in glycogen and nucleic acids	3
Heart	Ikoro	1616	Amide I (carbonyl stretching vibrations in side chains of amino acids)	3
		1215	PO$_2^-$ asymmetric (Phosphate I)	1
		1153	Stretching vibrations of hydrogen-bonding C–OH groups	1
		1069	CO-O-C symmetric stretching of phospholipids and cholesterol esters	3
		1022	Glycogen	1
		976	OCH$_3$ (polysaccharides, pectin)	1

		1701	Fatty acid esters	3
		1620	Peak of nucleic acids due to the base carbonyl stretching and ring breathing mode	3
	Gelegele	1570	Amide II	1
		1524	Stretching C=N, C=C	1
		1466	CH$_2$ scissoring mode of acyl chain of lipid, cholesterol-methyl band	1
		980	OCH$_3$ (polysaccharides-cellulose)	1
Kidney	Ikoro	1717	Amide I (arises from C=O stretching vibrations), C=O stretching vibrations DNA and RNA	1
		1678	Stretching C=O vibrations that are H-bonded (changes in the C=O stretching vibrations could be connected with destruction of old H-bonds and creation of the new ones).	1
		1616	Amide I (carbonyl stretching vibrations in side chains of amino acids)	3
		1543	Amide II	1
		1470	CH$_2$ bending of the methylene chains in lipids	1
		1204	Vibrational modes of collagen proteins-Amide III C–O–C, C–O dominated by the ring vibrations of polysaccharides C–O–P, P–O–P collagen	1
	Gelegele	1717	Amide I (arises from C=O stretching vibrations), C=O stretching vibrations DNA and RNA.	1
		1663	Amide I band, v(C=C) *cis*, lipids, fatty acids	3
		1597	C=N, NH$_2$ adenine	1
		1558	Ring base	1
		1524	Stretching C=N, C=C	1
		1466	CH$_2$ scissoring mode of the acyl chain of lipid	1
Liver	Ikoro	1751	v(C=C) lipids, fatty acids	3
		1443	δ(CH$_2$), lipids, fatty acids	1
		1366	Stretching C–O, deformation C–H, deformation N–H	1
		1219	PO$_2^-$ asymmetric vibrations of nucleic acids when it is highly hydrogen bonded, asymmetric hydrogen-bonded phosphate stretching mode	1

		Wavenumber	Assignment	Ref.
		1150	C–O stretching vibrations, C–O stretching mode of the carbohydrates CH_8	1
		1061	CO–O–C symmetric stretching of phospholipids and cholesterol esters	3
	Gelegele	1732	C=O stretching in lipids	1
		1639	Amide I	1
		1443	$\delta(CH_2)$, lipids, fatty acids, Asymmetric CH_3 bending of the methyl groups of proteins	3
		1551	Amide II of proteins, N–H bending and C–N stretching	1
		1470	CH_2 bending of the methylene chains in lipids	1
		1173	C–O (stretching in malignant tissues), non-hydrogen-bonded stretching mode of C–OH groups	1
	Ikoro	1740	>C=O ester stretching vibrations in triglycerides	3
		1659	Amide I	1
		1612	Amide I (carbonyl stretching vibrations in side chains of amino acids)	3
		1562	CO_2^- asymmetric stretching possibly from glutamic acid	2
		1504	In-plane CH bending vibrations from the phenyl rings	1
		1458	CH_3 asymmetric bending	2
Gills		1728	C=O band/ stretching	1, 2
		1651	80% C=O stretching; 10% C–N stretching; 10% N–H bending, Amide I absorption (predominantly the C=O stretching vibrations of the amide C=O)	1,2
	Gelegele	1589	Ring C–C stretch of phenyl, ring stretching vibrations with little interaction with CH in-plane bending	3
		1462	CH_2 scissoring	2
		1408	CH_3 asymmetric deformation, $(CH_3)_3N^+$ symmetric bending	1, 2
		1234	Amide III/phosphate vibrations of nucleic acids	1

- v: stretching, δ: deformation
- References: (1) Movasaghi et al. (2008); (2) Stuart (2005); (3) Obinaju et al. (2014)

Table 2 Attenuated total reflection Fourier-transform infrared (ATR-FTIR) spectroscopy distinguishing wavenumbers as shown in cluster vectors plots, and corresponding tentative chemical assignments: wavenumbers responsible for variance between tissue samples of the African catfish (*Heterobranchus bidorsalis*) obtained in March 2013 from sampling points Ifiayong, Ikoro and Gelegele in the Niger Delta region. Distinguishing wavenumbers were derived following the application of multivariate analysis using Ikoro as the reference site.

Sample	Site	Distinguishing wavenumbers (cm^{-1})	Tentative assignments	References
Brain	Ifiayong	1740	>C=O ester stretching vibrations in triglycerides	3
		1620	Peak of nucleic acids due to the base carbonyl stretching and ring breathing mode	3
		1501	In-plane CH bending vibrations from phenyl rings	1
		1142	Phosphate and oligosaccharides; oligosaccharide C–O bond in hydroxyl group that might interact with some other membrane components	1
		1030	Glycogen vibration; collagen and phosphodiester groups of nucleic acids; stretching C–O ribose	1
		961	C–O deoxyribose	1
	Gelegele	1728	C=O band/ stretching	1, 2
		1674	Anti-parallel β-sheet of Amide I, v(C=C) *trans*, lipids, fatty acids	1
		1234	Amide III/phosphate vibrations of nucleic acids	1
		1146	CO-O-C asymmetric stretching in glycogen and nucleic acids	3
		1034	Collagen	1
		964	C–C, C–O deoxyribose	1, 3
Heart	Ifiayong	1616	Amide I (carbonyl stretching vibrations in side chains of amino acids)	3
		1215	PO$_2^-$ asymmetric (Phosphate I)	1
		1153	Stretching vibrations of hydrogen-bonding C–OH groups	1
		1069	CO-O-C symmetric stretching of phospholipids and cholesterol esters	3
		1022	Glycogen	1
		976	OCH$_3$ (polysaccharides, pectin)	1
	Gelegele	1655	Amide I of proteins in α-helix conformation,	1

			Amide I (v C=O, δC–N, δN–H	
		1528	Stretching C=N, C=C	1
		1470	CH$_2$ bending of the methylene chains in lipids	1
		1273	CH$_\alpha$ rocking	1, 2
		1069	CO-O-C symmetric stretching of phospholipids and cholesterol esters	3
		1018	DNA ribose C‑O stretching RNA ribose C‑O stretching	2
Kidney	Ifiayong	1717	Amide I (arises from C=O stretching vibrations), C=O stretching vibrations DNA and RNA	1
		1678	Stretching C=O vibrations that are H-bonded (changes in the C=O stretching vibrations could be connected with destruction of old H-bonds and creation of the new ones)	1
		1616	Amide I (carbonyl stretching vibrations in side chains of amino acids)	3
		1543	Amide II	1
		1470	CH$_2$ bending of the methylene chains in lipids	1
		1204	Vibrational modes of collagen proteins-Amide III C–O–C, C–O dominated by the ring vibrations of polysaccharides C–O–P, P–O–P collagen	1
	Gelegele	1693	A high frequency vibration of an antiparallel β-sheet of Amide I (the Amide I band is due to in-plane stretching of the C=O band weakly coupled to stretching of the C–N and in-plane bending of the N–H bond	1
		1647	Amide I (α-helix)	2
		1612	Amide I (carbonyl stretching vibrations in side chains of amino acids)	3
		1543	Amide II	1
		1169	v_{as}CO–O–C	1
		1061	CO–O–C symmetric stretching of phospholipids and cholesterol esters	3
Liver	Ifiayong	1751	v(C=C) lipids, fatty acids	3
		1443	δ(CH$_2$), lipids, fatty acids	1
		1219	PO$_2^-$ asymmetric vibrations of nucleic acids when it is highly hydrogen bonded, asymmetric hydrogen-bonded	1

		phosphate stretching mode	
	1150	C–O stretching vibration, C–O stretching mode of the carbohydrates CH_8	1
	1061	CO–O–C symmetric stretching of phospholipids and cholesterol esters	3
	1732	C=O stretching in lipids	1
	1639	Amide I	1
	1508	In-plane CH bending vibrations from the phenyl rings	1
Gelegele	1470	CH_2 bending of the methylene chains in lipids	1
	1153	Stretching vibrations of hydrogen-bonding C–OH groups	1
	1057	Stretching C–O deoxyribose	1
	1740	>C=O ester stretching vibrations in triglycerides	3
	1659	Amide I	1
Ifiayong	1612	Amide I (Carbonyl stretching vibrations in side chains of amino acids)	3
	1562	CO_2^- asymmetric stretching possibly from glutamic acid	2
	1504	In-plane CH bending vibrations from the phenyl rings	1
	1458	CH_3 asymmetric bending	2
	1663	Amide I band, v(C=C) *cis*, lipids, fatty acids	3
	1589	Ring C–C stretch of phenyl	1
Gelegele	1543	Amide II (protein N-H bend, C-N stretch) in α-helices	3
	1462	CH_2 scissoring	2
	1178	C-O asymmetric stretching of glycogen	3
	968	C–C, C–O deoxyribose, DNA	1

(Note: "Gills" label appears in the leftmost column spanning the Ifiayong and Gelegele gill rows.)

- v: stretching, δ: deformation
- References: (1) Movasaghi et al. (2008); (2) Stuart (2005); (3) Obinaju et al. (2014)